Journal of Computational Physics 228 (2009) 9059–9078

Contents lists available at ScienceDirect

Journal of Computational Physics

journal homepage: www.elsevier.com/locate/jcp

A high order kinetic flux-vector splitting method for the reduced five-equation model of compressible two-fluid flows

Shamsul Qamar [a,b,*], Munshoor Ahmed [a]

[a] Department of Mathematics, COMSATS Institute of Information Technology, Plot No. 30, H-8/1 Islamabad, Pakistan
[b] Max Planck Institute for Dynamics of Complex Technical Systems, Sandtorstrasse 1, 39106 Magdeburg, Germany

ARTICLE INFO

Article history:
Received 20 April 2009
Received in revised form 4 September 2009
Accepted 9 September 2009
Available online 18 September 2009

MSC:
76T99
65Y99
65M99
35L45
35L65
35L67

Keywords:
Five-equation model
Kinetic flux-vector splitting schemes
Central schemes
Conservation laws
Hyperbolic systems
Shock solutions

ABSTRACT

We present a high order kinetic flux-vector splitting (KFVS) scheme for the numerical solution of a conservative interface-capturing five-equation model of compressible two-fluid flows. This model was initially introduced by Wackers and Koren (2004) [21]. The flow equations are the bulk equations, combined with mass and energy equations for one of the two fluids. The latter equation contains a source term in order to account for the energy exchange. We numerically investigate both one- and two-dimensional flow models. The proposed numerical scheme is based on the direct splitting of macroscopic flux functions of the system of equations. In two space dimensions the scheme is derived in a usual dimensionally split manner. The second order accuracy of the scheme is achieved by using MUSCL-type initial reconstruction and Runge–Kutta time stepping method. For validation, the results of our scheme are compared with those from the high resolution central scheme of Nessyahu and Tadmor [14]. The accuracy, efficiency and simplicity of the KFVS scheme demonstrate its potential for modeling two-phase flows.

1. Introduction

Two-fluid flow problems occur in various scientific and technical disciplines ranging from environmental research to modeling of operations in nuclear, chemical or processing engineering installations. The modeling and simulation of these flows is one of the most challenging problems in computational fluid dynamics. In such problems the flow regime of interest contains two or more non-mixed fluids separated by sharp interfaces. A challenging part in the numerical simulation of these models is the coupling of interface with the fluid flow model. Because, a coupling mismatch may introduce large errors in the numerical simulations.

In this manuscript, a conservative interface-capturing compressible two-fluid model of Wackers and Koren [21,22] is considered. In this model, instead of an explicit interface tracking procedure, the fluid is treated as a mixture of pure fluids in the vicinity of interface and reduces to a single fluid away from the interface. At the interface, there is a smooth but numerically

* Corresponding author. Address: Max Planck Institute for Dynamics of Complex Technical Systems, Sandtorstrasse 1, 39106 Magdeburg, Germany. Tel.: +49 391 6110454; fax: +49 391 6110500.
E-mail addresses: shamsul.qamar@comsats.edu.pk (S. Qamar), ahmed.manshoor@gmail.com (M. Ahmed).

0021-9991/$ - see front matter © 2009 Published by Elsevier Inc.
doi:10.1016/j.jcp.2009.09.010

smeared transition from one fluid to another. Hence, no additional equations are needed for capturing the behavior of flow in the interfacial cells. The interface motion is implicitly realized from the solution of the flow model. In one space dimension the model contains five equations. The equations include three bulk-fluid equations and mass and energy equations for one of the two pure fluids. A source term in the energy equation is responsible for the exchange of energy between the fluids. The energy exchange is only due to work; heat exchange between the two fluids is neglected. Because of the latter, the five-equation model of Wackers and Koren is not generally applicable. An extension of the Wackers and Koren model with a thermodynamic work term is given in a recent publication of Kreeft and Koren [8]. The source term can be integrated exactly through the shock wave, leading to an exact closure for the system in the case of discontinuous flow. The solution of this model needs no explicit algorithm for the interface motion. Hence, the model can be easily implemented in the existing flow solvers. Other interface-tracking models, such as the volume-of-fluid [6] and level-set [12,17] methods, require explicit equations for the interface motion.

In the literature, other two-phase flow models also exist for describing the behavior of physical mixtures. These models use separate pressures, velocities, and densities for each fluid. Moreover, a convection equation for the interface motion is coupled with the conservation laws of flow models. In the literature such models are known as seven-equation models. One of such models for solid–gas two-phase flows was initially introduced by Baer and Nunziato [3] and was further investigated by Abgrall and Saurel [1,16], among others.

In the current five-equation model, the explicit relations for primitive variables are only possible if both fluids satisfy the ideal-gas equations of state. For example, explicit relations are not possible if stiffened equation of state is used for one of the two fluids. It can be easily seen that the given model is not closed for this choice of the equation of state. There is another five-equation two-fluid flow model available in the literature [2,13]. In that model a separate convection equation for the interface motion is coupled with the flow models. As a results, the last energy equation for one of the two fluids, which is considered in the current model, disappears. Hence, the resulting two-fluid flow model is a homogeneous conservative hyperbolic system. In that model, one can use any equation of state and primitive variables can be explicitly determined from conservative variables.

Despite this limitation, the current model is more interesting to us due to the presence of differential source term in the energy equation for one of the two fluids. Similar source terms in the seven-equation models not only make the system non-conservative but also give a hard task to the numerical scheme. Such source terms, called nuzzling terms, appear in the models due to averaging. The solution of current reduced model with KFVS scheme will help us to understand the handling of nuzzling terms in the seven-equation models.

In the light of above discussion, the KFVS scheme is extended for solving one and two-dimensional two-fluid flow model of Wackers and Koren [21]. The proposed numerical scheme is based on the splitting of macroscopic flux functions of the system of equations of two-fluid flow model. The upwinding bias in numerical flux function can be naturally obtained by considering a fluid as a collection of particles. The movements of the particles in forward or backward directions automatically split the fluxes of mass, momentum and energy into forward and backward fluxes across the cell interface, i.e.

$$\mathbf{F}_{i+\frac{1}{2}} = \mathbf{F}^{+}(\mathbf{W}_i) + \mathbf{F}^{-}(\mathbf{W}_{i+1}),$$

where $\mathbf{W}_i$ represents a vector of mass, momentum and energy densities inside the cell $I_i := \left[x_{i-\frac{1}{2}}, x_{i+\frac{1}{2}}\right]$. In this scheme, we start with a cell averaged initial data of conservative variables and get back the cell averaged values of the conservative variables in the same cell at next time step. In the two-dimensional case, the flux splitting is done in a usual dimensionally split manner, that is, formula for the fluxes can be used along each coordinate direction. In order to get second-order accuracy, MUSCAL-type initial reconstruction and Runge–Kutta time stepping method are employed.

Kinetic flux-vector splitting (KFVS) schemes have been widely used for the flow simulations in gas dynamics. Mandal and Deshpande [10] have used KFVS schemes for the numerical solution of bump in a channel problem on structured meshes. Numerically, it was found in [10] that the explicit flux function of KFVS scheme, by employing collisionless Boltzmann transport equation, is similar to the flux function of van Leer [20]. The same result was first obtained by [5]. Moreover, Weatherill et al. [23] have used high order KFVS schemes for the simulation of several two-dimensional problems on structured and unstructured meshes. Recently, Xu [24] as well as Tang and Xu [18] have constructed an improved BGK-type kinetic flux-vector splitting scheme which also incorporate particle collisions at the cell interfaces. Furthermore, Tang et al. [19] and Xu [25] have implemented different KFVS schemes for solving shallow water equations.

For validation, the numerical results of the proposed KFVS scheme are compared with those from the central schemes [7,14]. These predictor–corrector type methods are applied in two steps. In the predictor step, the mid-point values are predicted by using a non-oscillatory piecewise-linear reconstructions of cell averages. In the second corrector step, staggered averaging, together with the predicted mid-values, are used to obtain the updated cell averaged solution. The second order accuracy in the schemes is achieved by employing MUSCL-type reconstruction procedure. Like the upwind schemes, the non-oscillatory nature of the scheme is guaranteed by using non-linear min-mod limiters. However, unlike the upwind schemes, the central schemes do not need the complicated time-consuming (approximate) Riemann solvers. This advantage is more attractive in the multi-dimensional cases where no exact Riemann solvers exist. Moreover, the central schemes are genuinely multi-dimensional because no dimensional splitting is required. The source term in the central schemes is approximated in the same manner as done by Liotta et al. [9] for relaxation-type hyperbolic conservation laws. A similar idea is also used in this article to approximate the source term in the KFVS scheme.

This article is organized as follows. In Section 2, the proposed one-dimensional two-fluid flow model is introduced. Afterwards, the one-dimensional KFVS scheme is derived for the numerical approximation of this model. We also briefly present the one-dimensional central scheme. In Section 3, the two-fluid flow model and corresponding numerical schemes are extended to two-space dimensions. In Section 4, numerical test problems are presented. Finally, Section 5 gives conclusions and remarks.

2. One-dimensional two-fluid flow model

In this section, we give a simplified compressible two-fluid flow model in which friction and heat conduction are neglected. For more details about the model the reader is referred to the report of Wackers and Koren [21,22].

In the derivation of this model, it is assumed that the whole domain of flow is filled with the mixture of two-fluids. In the macroscopic sense the fluid is a mixture, however on the microscopic level the two fluids retain their own properties. Moreover, both fluids have the same pressure and velocity. Hence, the fluids do not move relative to each other. The fluid elements interact each other by exerting forces on each other, thus exchanging work.

As mentioned before, a complete two-phase flow model has seven unknown variables containing, two densities, two velocities, two pressures and one variable describing the relative concentration of fluids. Such models contain seven equations, see [1,3,16]. However, the same velocity and pressure assumption for both fluids reduces the current model to five equations with five unknowns. Hence, the state vector $\mathbf{w}$ of primitive variables has the form $\mathbf{w} = (\rho_1, \rho_2, u, p, Y)^T$. Here, ρ_1 is a density of fluid 1, ρ_2 is a density of fluid 2, u is a bulk velocity, p is a bulk pressure and Y is a measure of the relative amount of fluid 1. To successfully integrate this model in time, we need five differential equations.

For bulk quantities, such as density ρ and total energy E, we assume that α is a volume fraction of fluid 1 which is chosen as the variable Y. This means that a part α of a small volume dV is filled with fluid 1 and a part $(1-\alpha)$ with fluid 2. Using these conventions, we can define

$$\rho = \alpha\rho_1 + (1-\alpha)\rho_2, \quad \rho E = \alpha\rho_1 E_1 + (1-\alpha)\rho_2 E_2 \tag{1}$$

and the total energy of each fluid as

$$E_1 = e_1 + \frac{1}{2}u^2, \quad E_2 = e_2 + \frac{1}{2}u^2, \tag{2}$$

where e_1 and e_2 denote the internal energies of fluids 1 and 2, respectively.

The one-dimensional two-fluid flow model according to Wackers and Koren [21,22] is given as

$$\mathbf{W}_t + \mathbf{F}(\mathbf{W})_x = \mathbf{S}, \tag{3a}$$

where

$$\mathbf{W} = \begin{pmatrix} \rho \\ \rho u \\ \rho E \\ \rho_1\alpha \\ \rho_1 E_1 \alpha \end{pmatrix}, \quad \mathbf{F}(\mathbf{W}) = \begin{pmatrix} \rho u \\ \rho u^2 + p \\ \rho u E + pu \\ \rho_1 u\alpha \\ \rho_1 E_1 u\alpha + pu\alpha \end{pmatrix}, \quad \mathbf{S} = \begin{pmatrix} 0 \\ 0 \\ 0 \\ 0 \\ s \end{pmatrix}. \tag{3b}$$

Here, $\mathbf{W}$ represents the vector of conservative variables, $\mathbf{F}$ is a vector of fluxes, and $\mathbf{S}$ is a vector of source terms with only last non-zero term.

2.1. Primitive variables

The system (3a) has five equations with seven unknowns $(\rho, \rho_1, u, p, e, e_1, \alpha)$. Therefore, further two equations are needed to close this system. This closure can be obtained by using the equations of state (EOS) required for describing the thermodynamic behavior of two fluids. As mentioned before, it is assumed that both fluid obey the ideal-gas equations of state. With this assumption, the relations for primitive variables are explicit. If both the fluids satisfy the ideal-gas law, i.e.

$$p = (\gamma - 1)\rho e \tag{4}$$

with constant γ representing the ratio of specific heats, then the total energies according to (1) and (2) are given as

$$\rho_1 E_1 \alpha = \frac{1}{\gamma_1 - 1} p\alpha + \frac{1}{2}\rho_1 \alpha u^2, \tag{5}$$

$$\rho_2 E_2 (1-\alpha) = \frac{1}{\gamma_2 - 1} p(1-\alpha) + \frac{1}{2}(\rho - \rho_1\alpha)u^2, \tag{6}$$

$$\rho E = \left(\frac{\alpha}{\gamma_1 - 1} + \frac{1-\alpha}{\gamma_2 - 1}\right)p + \frac{1}{2}\rho u^2. \tag{7}$$

Here, γ_1 and γ_2 are the ratio of specific heats for fluids 1 and 2, respectively. Rearranging Eqs. (5) and (6), we obtain after using (1)

$$p\alpha = (\gamma_1 - 1)\left((\rho_1 E_1 \alpha) - \frac{1}{2}\rho_1 \alpha u^2\right), \tag{8}$$

$$p(1-\alpha) = (\gamma_2 - 1)\left((\rho E) - (\rho_1 E_1 \alpha) - \frac{1}{2}(\rho - (\rho_1 \alpha))u^2\right). \tag{9}$$

By adding Eqs. (8) and (9), we get an expression for p, i.e.

$$p = (\gamma_1 - 1)\left((\rho_1 E_1 \alpha) - \frac{1}{2}(\rho_1 \alpha)u^2\right) + (\gamma_2 - 1)\left((\rho E) - (\rho_1 E_1 \alpha) - \frac{1}{2}(\rho - (\rho_1 \alpha))u^2\right). \tag{10}$$

After getting p, Eq. (8) can be used to obtain α as follows:

$$\alpha = \frac{(\gamma_1 - 1)\left((\rho_1 E_1 \alpha) - \frac{1}{2}(\rho_1 \alpha)u^2\right)}{p}. \tag{11}$$

Hence, all the primitive variables can be explicitly obtained from the conservative variable. The energy equations are directional independent, therefore for two-dimensional problem the procedure of calculating primitive variables remains the same. For two-fluid flows with $\gamma_1 = \gamma_2 = \gamma$, the terms $\rho_1 E_1 \alpha$ and $\rho_1 \alpha$ disappears from Eq. (10) and gives a reduced expression for p in the single-fluid

$$p = (\gamma - 1)\left(\rho E - \frac{1}{2}\rho u^2\right). \tag{12}$$

The source term s in the last equation of (3a) represents the transfer of energy from fluid 2 to fluid 1. We give here the final expression for the source term. For more details about the derivation of source term the reader is referred to Wackers and Koren [21,22]. The source term represents the exchange of energy into work. Both fluid elements move with the same velocity, therefore the velocity of the interface is equal to the velocity u of the fluid elements. Let us define the mass fraction of fluid 1 as

$$\beta = \frac{\rho_1 \alpha}{\rho}. \tag{13}$$

Then, the source term on the right-hand side of the energy equation for fluid 1 is given as

$$s = pu\alpha_x + (\alpha - \beta)up_x = u(p\alpha)_x - u\beta p_x. \tag{14}$$

With the above explicit expression for source term, the system in (3a) along with equations of states is closed.

2.2. One-dimensional kinetic flux-vector splitting scheme

In gas-kinetic theory, the flux is related to the particle motion across a cell interface. The numerical discretization of given system in (3a) corresponds to the evaluation of local macroscopic flux-vector $\mathbf{F}(\mathbf{W})$ through each boundary of the mesh cell. The particle motion in the x-direction determines the flux function. The remaining quantities, such as densities, pressure and volume fraction can be considered as passive scalars transporting with the particle velocity. Normally, particles are randomly distributed around the average velocity.

According to statistical mechanics, the distribution of moving particles along each coordinate direction can be described by local Maxwellian distribution. The Maxwellian distribution function f_M in the normal direction n is given as (e.g. [18])

$$f_M(t, n, v_n) = \rho\left(\frac{\lambda}{\pi}\right)^{\frac{1}{2}} \exp[-\lambda(u_n - v_n)^2], \quad \lambda = \frac{\rho}{2p}. \tag{15}$$

In the one-dimensional case $n \in x$ and in the two-dimensional case $n \in \{x, y\}$. In other words, we can use the same distribution for both one- and two-dimensional flows, see, for example [18]. The transport of any flow quantity is due to the movement of particles. Let us consider the one-dimensional flow. With the distribution function f_M in (15), one can split the particles into two groups. One group is moving to the right with positive velocity ($u_n > 0$) and the other group is moving to the left with negative velocity ($u_n < 0$). Before splitting the fluxes, let us define

$$\langle v^0 \rangle_n = 1 = \int_{-\infty}^{\infty} \left(\frac{\lambda}{\pi}\right)^{\frac{1}{2}} e^{-\lambda(u_n - v_n)^2} dv_n, \tag{16}$$

$$\langle v^1 \rangle_n = u_n = \int_{-\infty}^{\infty} \left(\frac{\lambda}{\pi}\right)^{\frac{1}{2}} v_n e^{-\lambda(u_n - v_n)^2} dv_n. \tag{17}$$

The above two moments are sufficient to split all the fluxes. In order to simplify the notation, we define

$$\langle v^0\rangle_{+n} = \int_0^\infty \left(\frac{\lambda}{\pi}\right)^{\frac{1}{2}} e^{-\lambda(u_n-v_n)^2} dv_n = \frac{1}{2}\operatorname{erfc}(-\sqrt{\lambda}u_n), \tag{18}$$

$$\langle v^0\rangle_{-n} = \int_{-\infty}^0 \left(\frac{\lambda}{\pi}\right)^{\frac{1}{2}} e^{-\lambda(u_n-v_n)^2} dv_n = \frac{1}{2}\operatorname{erfc}(\sqrt{\lambda}u_n) \tag{19}$$

and

$$\langle v^1\rangle_{+n} = \int_0^\infty \left(\frac{\lambda}{\pi}\right)^{\frac{1}{2}} v_n e^{-\lambda(u_n-v_n)^2} dv_n = u_n\langle v^0\rangle_{+n} + \frac{1}{2}\frac{e^{-\lambda u_n^2}}{\sqrt{\pi\lambda}}, \tag{20}$$

$$\langle v^1\rangle_{-n} = \int_{-\infty}^0 \left(\frac{\lambda}{\pi}\right)^{\frac{1}{2}} v_n e^{-\lambda(u_n-v_n)^2} dv_n = u_n\langle v^0\rangle_{-n} - \frac{1}{2}\frac{e^{-\lambda u_n^2}}{\sqrt{\pi\lambda}}. \tag{21}$$

In the above equations, the positive sign represents those particles moving in the positive (right) direction and the negative sign represents the particles moving in the negative (left) direction. Moreover, the complementary error function is defined as

$$\operatorname{erfc}(z) = \frac{2}{\sqrt{\pi}}\int_z^\infty e^{-t^2} dt. \tag{22}$$

With the help of above flux-splitting technique, we can derive a KFVS scheme for solving (3a).

In order to apply a finite volume scheme, the first step is to subdivide the domain of interest into N sub-domains or mesh cells. Let us define the cell I_i by interval $\left[x_{i-\frac{1}{2}}, x_{i+\frac{1}{2}}\right]$ for $i = 1, 2, \cdots, N$. Therefore, $\Delta x = x_{i+\frac{1}{2}} - x_{i-\frac{1}{2}}$ represents the uniform cells width, the points $x_i = i\Delta x$ refer to the cells center and the points $x_{i\pm 1/2} = x_i \pm \Delta x/2$ represent the cells faces. We start with a cell averaged initial data $\mathbf{W}_i^n$ at time step t^n and compute the cell average updated solution $\mathbf{W}_i^{n+1}$ over the same cells at the next time step t^{n+1}. This is performed easily by assuming the CFL condition

$$\Delta t \leqslant \Delta x\left(\frac{1}{\max(|v_i| + c_i)}\right), \tag{23}$$

where the speed of sound according to Wackers and Koren [21] is given as $c_i = \sqrt{(\alpha\gamma_1 + (1-\alpha)\gamma_2)p_i/\rho_i}$. After having the above definitions, we are ready to split the flux functions in (3a) as

$$\mathbf{F}(\mathbf{W}) = \begin{pmatrix} \rho u \\ \rho u^2 + p \\ \rho u E + p u \\ \rho_1 u\alpha \\ \rho_1 E_1 u\alpha + p u\alpha \end{pmatrix} = \mathbf{F}^+ + \mathbf{F}^-, \tag{24}$$

where

$$\mathbf{F}^\pm = \langle v^1\rangle_{\pm x}\begin{pmatrix} \rho \\ \rho u \\ \rho E + \frac{1}{2}p \\ \rho_1\alpha \\ \rho_1 E_1\alpha + \frac{1}{2}p\alpha \end{pmatrix} + \langle v^0\rangle_{\pm x}\begin{pmatrix} 0 \\ p \\ \frac{1}{2}pu \\ 0 \\ \frac{1}{2}pu\alpha \end{pmatrix}. \tag{25}$$

Therefore, the flux-vector at the right interface of the cell I_i is given as

$$\mathbf{F}_{i+\frac{1}{2}} = \mathbf{F}_i^+ + \mathbf{F}_{i+1}^-. \tag{26}$$

Analogously, we can define the left interface flux-vector of the cell I_i. The integration of the (3a) over the cell $I_i = \left[x_{i-\frac{1}{2}}, x_{i+\frac{1}{2}}\right]$ gives the following semi-discrete kinetic upwind scheme:

$$\frac{d\mathbf{W}_i}{dt} = -\frac{\mathbf{F}_{i+\frac{1}{2}} - \mathbf{F}_{i-\frac{1}{2}}}{\Delta x} + \frac{1}{\Delta x}\int_{x_{i-\frac{1}{2}}}^{x_{i+\frac{1}{2}}} \mathbf{S}(\mathbf{W})dx, \tag{27}$$

where the cell averaged value $\mathbf{W}_i$ is defined as

$$\mathbf{W}_i := \mathbf{W}_i(t) = \frac{1}{\Delta x}\int_{x_{i-\frac{1}{2}}}^{x_{i+\frac{1}{2}}} \mathbf{W}(t,x)dx \tag{28}$$

and $\mathbf{F}_{i+\frac{1}{2}}$ is given by (26).

As a next step, we approximate the source term on the right-hand side of (27). In Eq. (3a), the source vector has only one non-zero component which is given by (14). By using KFVS scheme, this component can be approximated in the following manner:

$$\int_{x_{i-\frac{1}{2}}}^{x_{i+\frac{1}{2}}} s dx = \int_{x_{i-\frac{1}{2}}}^{x_{i+\frac{1}{2}}} (u(p\alpha)_x - u\beta p_x) dx = u_i\Big((p\alpha)_{i+\frac{1}{2}} - (p\alpha)_{i-\frac{1}{2}}\Big) - (u\beta)_i\Big(p_{i+\frac{1}{2}} - p_{i-\frac{1}{2}}\Big) = s_{i+\frac{1}{2}} - s_{i-\frac{1}{2}}, \tag{29}$$

where u_i and $(u\beta)_i$ are the averaged values at the centroid of cell I_i and $s_{i\pm\frac{1}{2}}$ are the source term fluxes at the interfaces of the cell I_i. They are defined as

$$s_{i\pm\frac{1}{2}} = u_i(p\alpha)_{i\pm\frac{1}{2}} - (u\beta)_i p_{i\pm\frac{1}{2}}, \tag{30}$$

where at the right interface of cell I_i, we have

$$(p\alpha)_{i+\frac{1}{2}} = (p\alpha)_i^+ + (p\alpha)_{i+1}^-, \quad p_{i+\frac{1}{2}} = p_i^+ + p_{i+1}^-. \tag{31}$$

Similarly, one can obtain the left interface values. The splitting procedure is analogous to that presented in (24)–(26) for cell interface fluxes.

Hence, the semi-discrete scheme (27) can be re-written as

$$\frac{d\mathbf{W}_i}{dt} = -\frac{\mathbf{F}_{i+\frac{1}{2}} - \mathbf{F}_{i-\frac{1}{2}}}{\Delta x} + \frac{1}{\Delta x}\Big(\mathbf{S}_{i+\frac{1}{2}} - \mathbf{S}_{i-\frac{1}{2}}\Big). \tag{32}$$

Only the last component of vectors $\mathbf{S}_{i\pm\frac{1}{2}}$ are non-zero as given by (30).

The above scheme is first order accurate in space. To achieve high order accuracy, the initial reconstruction strategy must be applied for interpolating the cell averaged variables $\mathbf{W}_i$. Here, a second order accurate MUSCL-type initial reconstruction procedure is employed. Starting with a piecewise-constant solution, $\mathbf{W}_i$, one reconstruct a piecewise linear (MUSCL-type) approximation in x-directions by selecting the slope vector (differences) $\mathbf{W}^x$. The boundary extrapolated values are given as

$$\mathbf{W}_i^L = \mathbf{W}_i - \frac{1}{2}\mathbf{W}_i^x, \quad \mathbf{W}_i^R = \mathbf{W}_i + \frac{1}{2}\mathbf{W}_i^x.$$

A possible computation of these slopes, is given by family of *discrete derivatives* parameterized with $1 \leqslant \theta \leqslant 2$, for example

$$\mathbf{W}_i^x = MM\Big\{\theta\Delta\mathbf{W}_{i+\frac{1}{2}}, \frac{\theta}{2}\Big(\Delta\mathbf{W}_{i+\frac{1}{2}} + \Delta\mathbf{W}_{i-\frac{1}{2}}\Big), \theta\Delta\mathbf{W}_{i-\frac{1}{2}}\Big\}, \tag{33}$$

where $1 \leqslant \theta \leqslant 2$ is a parameter and Δ denotes central differencing,

$$\Delta\mathbf{W}_{i+\frac{1}{2}} = \mathbf{W}_{i+1} - \mathbf{W}_i.$$

Here *MM* denotes the min-mod non-linear limiter

$$MM\{x_1, x_2, \ldots\} = \begin{cases} \min_i\{x_i\} & \text{if } x_i > 0 \quad \forall i, \\ \max_i\{x_i\} & \text{if } x_i < 0 \quad \forall i, \\ 0 & \text{otherwise.} \end{cases} \tag{34}$$

On the basis of above reconstruction, a semi-discrete high resolution kinetic solver is given as

$$\frac{d\mathbf{W}_i}{dt} = -\frac{\mathbf{F}_{i+\frac{1}{2}}(\mathbf{W}_{i+1}^L, \mathbf{W}_i^R) - \mathbf{F}_{i-\frac{1}{2}}(\mathbf{W}_i^L, \mathbf{W}_{i-1}^R)}{\Delta x} + \frac{\mathbf{S}_{i+\frac{1}{2}}(\mathbf{W}_{i+1}^L, \mathbf{W}_i^R) - \mathbf{S}_{i-\frac{1}{2}}(\mathbf{W}_i^L, \mathbf{W}_{i-1}^R)}{\Delta x}. \tag{35}$$

To obtain second order accuracy in time, we use a second order TVD Runge–Kutta scheme to solve (35). Denoting the right-hand side of (35) as $L(\mathbf{W})$, a second order TVD Runge–Kutta scheme update $\mathbf{W}$ through the following two stages (see e.g. [18])

$$\mathbf{W}^{(1)} = \mathbf{W}^n + \Delta t L(\mathbf{W}^n), \tag{36a}$$

$$\mathbf{W}^{n+1} = \frac{1}{2}(\mathbf{W}^n + \mathbf{W}^{(1)} + \Delta t L(\mathbf{W}^{(1)})), \tag{36b}$$

where $\mathbf{W}^n$ is a solution at previous time step and $\mathbf{W}^{n+1}$ is updated solution at next time step. Moreover, Δt represents the time step.

2.3. One-dimensional central schemes

In order to validate the results of KFVS scheme, we extend the high-resolution non-oscillatory central schemes of Nessyahu and Tadmor [14] for the solution of current two-fluid flow model. These predictor–corrector type methods are applied in two steps. In the predictor step, the mid-point values are predicted by using the non-oscillatory piecewise-linear recon-

structions of the cell averages. In the second corrector step, staggered averaging, together with the predicted mid-values, are used to obtain the updated cell averaged solution. The source term in the central schemes is approximated in the same manner as done by Liotta et al. [9] for relaxation-type hyperbolic conservation laws. In summary, the scheme can be presented as

$$\text{Predictor}: \ \mathbf{W}_i^{n+\frac{1}{2}} = \mathbf{W}_i^n - \frac{\xi}{2}\mathbf{F}^x(\mathbf{W}_i^n) + \frac{\xi}{2}\mathbf{S}^x(\mathbf{W}_i^n), \tag{37}$$

$$\text{Corrector}: \ \mathbf{W}_{i+\frac{1}{2}}^{n+1} = \frac{1}{2}(\mathbf{W}_i^n + \mathbf{W}_{i+1}^n) + \frac{1}{8}(\mathbf{W}_i^x - \mathbf{W}_{i+1}^x) - \xi\left[\mathbf{F}_{i+1}^{n+\frac{1}{2}} - \mathbf{F}_i^{n+\frac{1}{2}}\right] + \xi\left[\mathbf{S}_{i+1}^{n+\frac{1}{2}} - \mathbf{S}_i^{n+\frac{1}{2}}\right], \tag{38}$$

where $\xi = \Delta t/\Delta x$. The non-zero component of source vector in (38), according to (14), is given as

$$s_{i+1}^{n+\frac{1}{2}} - s_i^{n+\frac{1}{2}} = \frac{1}{2}\left(u_i^{n+\frac{1}{2}} + u_{i+1}^{n+\frac{1}{2}}\right)\left((p\alpha)_{i+1}^{n+\frac{1}{2}} - (p\alpha)_i^{n+\frac{1}{2}}\right) - \frac{1}{2}\left((u\beta)_i^{n+\frac{1}{2}} + (u\beta)_{i+1}^{n+\frac{1}{2}}\right)\left(p_{i+1}^{n+\frac{1}{2}} - p_i^{n+\frac{1}{2}}\right). \tag{39}$$

Moreover, $\frac{1}{\Delta x}\mathbf{F}^x(\mathbf{W}_i)$ stands for an approximate numerical derivatives of the flux $\mathbf{F}(t, x = x_i)$

$$\frac{1}{\Delta x}\mathbf{F}^x(\mathbf{W}_i) = \frac{\partial}{\partial x}\mathbf{F}(w(t, x = x_i) + O(\Delta x). \tag{40}$$

Analogously, $\mathbf{S}^x(\mathbf{W}_i)$ can be defined. Like $\mathbf{W}_i^x$ in (33), the fluxes $\mathbf{F}^x(\mathbf{W}_i)$ are computed by applying the min-mod limiter to each of the component of $\mathbf{F}$. Moreover, $\mathbf{S}^x(\mathbf{W}_i)$ can be obtained from the already calculated values of $\mathbf{W}_i^x$. This componentwise approach is one of the main advantages offered by central schemes over corresponding characteristic decompositions required by upwind schemes.

3. Two-dimensional two-flow flow model

In two-space dimensions the two-fluid flow model of six equations is given as

$$\mathbf{W}_t + \mathbf{F}(\mathbf{W})_x + \mathbf{G}(W)_y = \mathbf{Q} + \mathbf{R}, \tag{41a}$$

where $\mathbf{Q}$ and $\mathbf{R}$ are source term effects along x- and y-coordinate directions:

$$\mathbf{W} = (\rho, \rho u, \rho v, \rho E, \rho_1\alpha, \rho_1 E_1\alpha)^T, \tag{41b}$$

$$\mathbf{F} = (\rho u, \rho u^2 + p, \rho uv, \rho uE + pu, \rho_1 u\alpha, (\rho_1 E_1\alpha + p\alpha)u)^T, \tag{41c}$$

$$\mathbf{G} = (\rho v, \rho uv, \rho v^2 + p, \rho vE + pv, \rho_1 v\alpha, (\rho_1 E_1\alpha + p\alpha)v)^T, \tag{41d}$$

$$\mathbf{Q} = (0,0,0,0,0,s_x)^T, \quad \mathbf{R} = (0,0,0,0,0,s_y)^T. \tag{41e}$$

As mentioned before, the energy equation are directional independent, therefore for one- and two-dimensional problems the procedure of calculating primitive variables is same. For the two-dimensional case, however, we briefly explain them again. Let $|\mathbf{u}| := \sqrt{u^2 + v^2}$. The total energies of fluids 1 and 2 are given as

$$\rho_1 E_1\alpha = \frac{1}{\gamma_1 - 1}p\alpha + \frac{1}{2}\rho_1\alpha|\mathbf{u}|^2, \tag{42}$$

$$\rho_2 E_2(1-\alpha) = \frac{1}{\gamma_2 - 1}p(1-\alpha) + \frac{1}{2}(\rho - \rho_1\alpha)|\mathbf{u}|^2. \tag{43}$$

On adding the above two equations, we obtain the total bulk energy

$$\rho E = \left(\frac{\alpha}{\gamma_1 - 1} + \frac{1-\alpha}{\gamma_2 - 1}\right)p + \frac{1}{2}\rho|\mathbf{u}|^2. \tag{44}$$

Moreover, the expressions for the pressure and volume fraction are given as

$$p = (\gamma_1 - 1)\left(\rho_1 E_1\alpha - \frac{1}{2}\rho_1\alpha|\mathbf{u}|^2\right) + (\gamma_2 - 1)\left(\rho E - \rho_1 E_1\alpha - \frac{1}{2}(\rho - (\rho_1\alpha))|\mathbf{u}|^2\right), \tag{45}$$

$$\alpha = \frac{(\gamma_1 - 1)\left((\rho_1 E_1\alpha) - \frac{1}{2}(\rho_1\alpha)|\mathbf{u}|^2\right)}{p}. \tag{46}$$

Analogously, the components of source vectors in (41e) are given as

$$s_x = u((p\alpha)_x - \beta p_x), s_y = v((p\alpha)_y - \beta p_y). \tag{47}$$

3.1. Two-dimensional KFVS scheme

In order to solve (41) numerically, we discretize the given computational domain. Let N_x and N_y be large integers in the x- and y-directions, respectively. We assume a Cartesian grid with a rectangular domain $[0, x_{\max}] \times [0, y_{\max}]$ which is covered

by cells $C_{ij} \equiv \left[x_{i-\frac{1}{2}}, x_{i+\frac{1}{2}}\right] \times \left[y_{j-\frac{1}{2}}, y_{j+\frac{1}{2}}\right]$ for $1 \leqslant i \leqslant N_x$ and $1 \leqslant j \leqslant N_y$. The representative coordinates of the cell C_{ij} are denoted by (x_i, y_j). In each cell C_{ij} we use the cell averaged values of conservative variables

$$\mathbf{W}_{i,j}(t) = \mathbf{W}(t, x_i, y_j) = \frac{1}{\Delta x \Delta y} \int_{x_{i-\frac{1}{2}}}^{x_{i+\frac{1}{2}}} \int_{y_{j-\frac{1}{2}}}^{y_{j+\frac{1}{2}}} \mathbf{W}(t, x, y) dy\, dx. \tag{48}$$

Integration of Eq. (41a) over control volume $\left[x_{i-\frac{1}{2}}, x_{i+\frac{1}{2}}\right] \times \left[y_{i-\frac{1}{2}}, y_{j+\frac{1}{2}}\right]$ gives

$$\frac{d\mathbf{W}_{i,j}}{dt} = -\frac{1}{\Delta x}\left[\mathbf{F}_{i+\frac{1}{2}j} - \mathbf{F}_{i-\frac{1}{2}j}\right] - \frac{1}{\Delta y}\left[\mathbf{G}_{ij+\frac{1}{2}} - \mathbf{G}_{ij-\frac{1}{2}}\right] + \frac{1}{\Delta x \Delta y} \int_{x_{i-\frac{1}{2}}}^{x_{i+\frac{1}{2}}} \int_{y_{j-\frac{1}{2}}}^{y_{j+\frac{1}{2}}} [\mathbf{Q}(t, x, y) + \mathbf{R}(t, x, y)] dy\, dx, \tag{49}$$

where

$$\mathbf{F}_{i+\frac{1}{2}j} = \mathbf{F}^{+}_{ij} + \mathbf{F}^{-}_{i+1\,j}, \quad \mathbf{G}_{ij+\frac{1}{2}} = \mathbf{G}^{+}_{ij} + \mathbf{G}^{-}_{ij+1}. \tag{50}$$

The splitting of above fluxes can be obtained along each coordinate direction in a manner similar to the one-dimensional case. In this case, the flux-vector **F** at the cell interfaces perpendicular to the x-axis is split according to the x-component of the velocity denoted by u and the flux-vector **G** at the cell interfaces perpendicular to the y-axis is split according to the y-component of velocity represented by v.

The source term integrals in (49) can be approximated in the same manner as in the one-dimensional case. They are given as

$$\int_{x_{j-\frac{1}{2}}}^{x_{j+\frac{1}{2}}} \int_{y_{j-\frac{1}{2}}}^{y_{j+\frac{1}{2}}} s_x(t, x, y) dy\, dx = \Delta y\left[(s_x)_{i+\frac{1}{2}j} - (s_x)_{i-\frac{1}{2}j}\right], \tag{51}$$

$$\int_{x_{j-\frac{1}{2}}}^{x_{j+\frac{1}{2}}} \int_{y_{j-\frac{1}{2}}}^{y_{j+\frac{1}{2}}} s_x(t, x, y) dy\, dx = \Delta x\left[(s_y)_{ij+\frac{1}{2}} - (s_y)_{ij-\frac{1}{2}}\right], \tag{52}$$

where

$$(s_x)_{i\pm\frac{1}{2}j} = u_{i,j}(p\alpha)_{i+\frac{1}{2}j} - (u\beta)_{i,j} p_{i+\frac{1}{2}j} \tag{53}$$

$$(s_y)_{ij\pm\frac{1}{2}} = v_{ij}(p\alpha)_{ij\pm\frac{1}{2}} - (v\beta)_{ij} p_{ij\pm\frac{1}{2}}. \tag{54}$$

Here, $u_{i,j}$, $v_{i,j}$, $(u\beta)_{i,j}$ and $(v\beta)_{i,j}$ represent cell average values in the cell C_{ij}. Due to Eqs. (51) and (52), the two-dimensional semi-discrete KFVS scheme (49) can be rewritten as

$$\frac{d\mathbf{W}_{i,j}}{dt} = -\frac{1}{\Delta x}\left[\mathbf{F}_{i+\frac{1}{2}j} - \mathbf{F}_{i-\frac{1}{2}j}\right] - \frac{1}{\Delta y}\left[\mathbf{G}_{ij+\frac{1}{2}} - \mathbf{G}_{ij-\frac{1}{2}}\right] + \frac{1}{\Delta x}\left[\mathbf{Q}_{i+\frac{1}{2}j} - \mathbf{Q}_{i-\frac{1}{2}j}\right] + \frac{1}{\Delta y}\left[\mathbf{R}_{ij+\frac{1}{2}} - \mathbf{R}_{ij-\frac{1}{2}}\right]. \tag{55}$$

Similar to the one-dimensional case, only last components of **Q** and **R** are non-zero. This scheme is only first accurate in space. The second order accuracy of the scheme along each coordinate direction follows the same procedure as explained in the one-dimensional case. To obtain second order accuracy in time, the second order TVD Runge–Kutta scheme (36b) is used.

4. Two-dimensional central scheme

The two-dimensional central schemes was proposed by Jaing and Tadmor [7]. The scheme has a two-step predictor–corrector form. Starting with the cell averages, $\mathbf{W}^{n}_{ij}$, we use the first-order predictor step for the evolution of the mid-point values, $\mathbf{W}^{n+\frac{1}{2}}_{i,j}$, followed by the second-order corrector step for computation of the new cell averages $\mathbf{W}^{n+1}_{i,j}$. Like the one-dimensional case, no exact (approximate) Riemann solvers are needed. The non-oscillatory behavior of the scheme is dependent on the reconstructed discrete slopes, $\mathbf{W}^{x}$, $\mathbf{W}^{y}$, $\mathbf{F}^{x}(w)$, and $\mathbf{G}^{y}(w)$. At each time step the grid is staggered to avoid the flux calculation at the cell interfaces. The scheme is summarized below.

In the predictor step one has to calculate the mid-point values by using

$$\mathbf{W}^{n+\frac{1}{2}}_{i,j} = \mathbf{W}^{n}_{i,j} - \frac{\xi}{2}\mathbf{F}^{x}\left(\mathbf{W}^{n}_{i,j}\right) - \frac{\eta}{2}\mathbf{G}^{y}\left(\mathbf{W}^{n}_{i,j}\right) + \frac{\xi}{2}\mathbf{S}^{x}(\mathbf{W}^{n}_{i,j}) + \frac{\eta}{2}\mathbf{S}^{y}(\mathbf{W}^{n}_{i,j}). \tag{56}$$

where $\xi = \Delta t/\Delta x$ and $\eta = \Delta t/\Delta y$. This step is followed by a corrector step to get the updated values at the next time step by using

$$\mathbf{W}^{n+1}_{i+\frac{1}{2}j+\frac{1}{2}} = \frac{1}{4}\left(\mathbf{W}^{n}_{ij} + \mathbf{W}^{n}_{i+1j} + \mathbf{W}^{n}_{ij+1} + \mathbf{W}^{n}_{i+1j+1}\right) + \frac{1}{16}\left(\mathbf{W}^{x}_{ij} - \mathbf{W}^{x}_{i+1j}\right) - \frac{\xi}{2}\left(\mathbf{F}^{n+\frac{1}{2}}_{i+1j} - \mathbf{F}^{n+\frac{1}{2}}_{ij}\right) + \frac{1}{16}\left(\mathbf{W}^{x}_{ij+1} - \mathbf{W}^{x}_{i+1j+1}\right)$$
$$- \frac{\xi}{2}\left(\mathbf{F}^{n+\frac{1}{2}}_{i+1j+1} - \mathbf{F}^{n+\frac{1}{2}}_{ij+1}\right) + \frac{1}{16}\left(\mathbf{W}^{y}_{ij} - \mathbf{W}^{y}_{ij+1}\right) - \frac{\eta}{2}\left(\mathbf{G}^{n+\frac{1}{2}}_{ij+1} - \mathbf{G}^{n+\frac{1}{2}}_{ij}\right) + \frac{1}{16}\left(\mathbf{W}^{y}_{i+1j} - \mathbf{W}^{y}_{i+1j+1}\right)$$
$$- \frac{\eta}{2}\left(\mathbf{G}^{n+\frac{1}{2}}_{i+1j+1} - \mathbf{G}^{n+\frac{1}{2}}_{i+1j}\right) + \frac{\xi}{2}\left(\mathbf{Q}^{n+\frac{1}{2}}_{i+1j} - \mathbf{Q}^{n+\frac{1}{2}}_{ij}\right) + \frac{\xi}{2}\left(\mathbf{Q}^{n+\frac{1}{2}}_{i+1j+1} - \mathbf{Q}^{n+\frac{1}{2}}_{ij+1}\right) + \frac{\eta}{2}\left(\mathbf{R}^{n+\frac{1}{2}}_{ij+1} - \mathbf{R}^{n+\frac{1}{2}}_{ij}\right)$$
$$+ \frac{\eta}{2}\left(\mathbf{R}^{n+\frac{1}{2}}_{i+1j+1} - \mathbf{R}^{n+\frac{1}{2}}_{i+1j}\right). \tag{57}$$

The approximation of the non-zero source differences in the above equation follow the same procedure as given in (39).

5. Numerical test problems

In this section, we present six numerical test problems in order to validate the application of KFVS schemes for the simulation of two-fluid flow problems. For comparison, we use the results of high resolution central schemes [7,14] presented in the previous section.

5.1. One-dimensional test problems

Here, we present four one-dimensional shock tube problems. The exact solutions, represented by continuous lines, are obtained by using the same KFVS scheme on very refined mesh. The dashed lines represent the solution of KFVS scheme, while doted lines are used for representing the results of central scheme.

Problem 1 (*Translating two-fluid interface*). The initial data are given as

$$(\rho, u, p, \alpha) = (1000, 1, 1, 1), \quad \text{if } x \leqslant 0.25, \tag{58}$$
$$(\rho, u, p, \alpha) = (1, 1, 1, 0), \quad \text{if } x > 0.25. \tag{59}$$

The ratio of specific heats are given as $\gamma_L = 1.4$ and $\gamma_R = 1.6$. We have chosen 200 mesh cells and the final simulation time is $t = 0.1$. This problem is a contact discontinuity of water–air density ratio. The numerical results are shown in Fig. 2. The same problem was also considered in [8,21]. In this problem, both pressure and velocity are the same. Therefore, the interface is moving to the right with uniform speed and pressure. The numerical results show that KFVS scheme resolves the two-fluid interface very well as compared to the central scheme. Moreover, both velocity and pressure profiles are oscillation free.

Problem 2. This problem is analogous to the Sod's problem in the single phase gas dynamics which was also studied in [21]. Here, the density and pressure ratios are larger and the left gas and right gas have different ratios of specific heats. Both gases are separated by a very thin membrane located at $x = 0.5$. The gases on both sides of the membrane are at rest. The left side gas has high density and pressure compared to that on the right side of the membrane. After removing the membrane, the gases evolution in time take place. The initial data are given as

$$(\rho, u, p, \alpha) = (10, 0, 10, 1), \quad \text{if } x \leqslant 0.5 \tag{60}$$
$$(\rho, u, p, \alpha) = (0.125, 0, 0.1, 0), \quad \text{if } x > 0.5. \tag{61}$$

The ratio of specific heats for the left and right side gases are taken as $\gamma_L = 1.4$ and $\gamma_R = 1.6$, respectively. The numerical results at $t = 0.015$ are shown in Figs. 3 and 4. The solution contains a left-going rarefaction wave, right-going shock wave and the right-moving two-fluid interface. In Fig. 3, the solutions of KFVS and central scheme are compared at 300 mesh cells. The exact solution is obtained from the same KFVS scheme at very refined mesh. Both schemes give correct location of the discontinuities. Moreover, no pressure oscillations are observed in the solution. Finally, Fig. 4 shows the zoomed plots of density and pressure. The results show that KFVS scheme resolve the sharp discontinuities better than the central scheme.

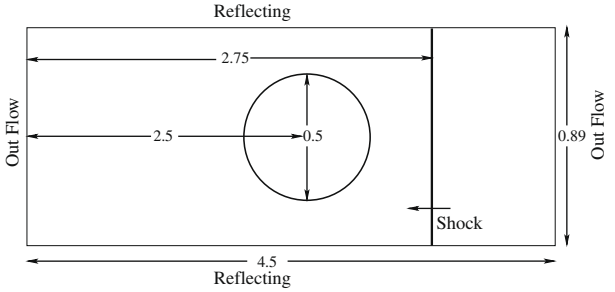

Fig. 1. Sketch of computational domain.

Problem 3. The initial data are given as

$$(\rho, u, p, \alpha) = (2.0, 0, 1000, 1), \quad \text{if } x \leqslant 0.5 \tag{62}$$
$$(\rho, u, p, \alpha) = (1, 0, 0.01, 0), \quad \text{if } x > 0.5. \tag{63}$$

The ratio of specific heats are given as $\gamma_L = 1.4$ and $\gamma_R = 1.2$. This is a very hard test problem for a numerical scheme. The solution contain a left moving rarefaction wave, a contact discontinuity, and a right moving shock wave. The right moving shock hits the interface at $x = 0.5$. The shock continues to move towards right and a rarefaction wave is created which is moving towards left. We choose 500 mesh cells and the final simulation time is taken as $t = 0.012$. The numerical results are shown in Figs. 5 and 6. The figures show that both schemes give comparable results.

Problem 4 (*No-reflection problem*). The initial data are given as

$$(\rho, u, p, \alpha) = (3.1748, 9.435, 100, 1), \quad \text{if } x \leqslant 0.5, \tag{64}$$
$$(\rho, u, p, \alpha) = (1, 0, 1, 0), \quad \text{if } x > 0.5. \tag{65}$$

The ratio of specific heats are given as $\gamma_L = 1.667$ and $\gamma_R = 1.2$. We have chosen 400 mesh cells and the final simulation time is $t = 0.02$. This is also a hard test problem for a numerical scheme with large jumps in the pressure at the interface. The choice of pressure and velocity jump over the shock prevents the creation of a reflection wave. Therefore, a shock wave moves to the right. The numerical results are shown in Fig. 7. The results of KFVS scheme seems to be superior than the central scheme. Moreover, wiggles are visible in the velocity and pressure plots of both schemes, representing small waves that are reflected to the left. However, unlike real velocity and pressure oscillations, these wiggles reduces in size on refined mesh. Similar wiggles are also visible in the results presented in [8,21].

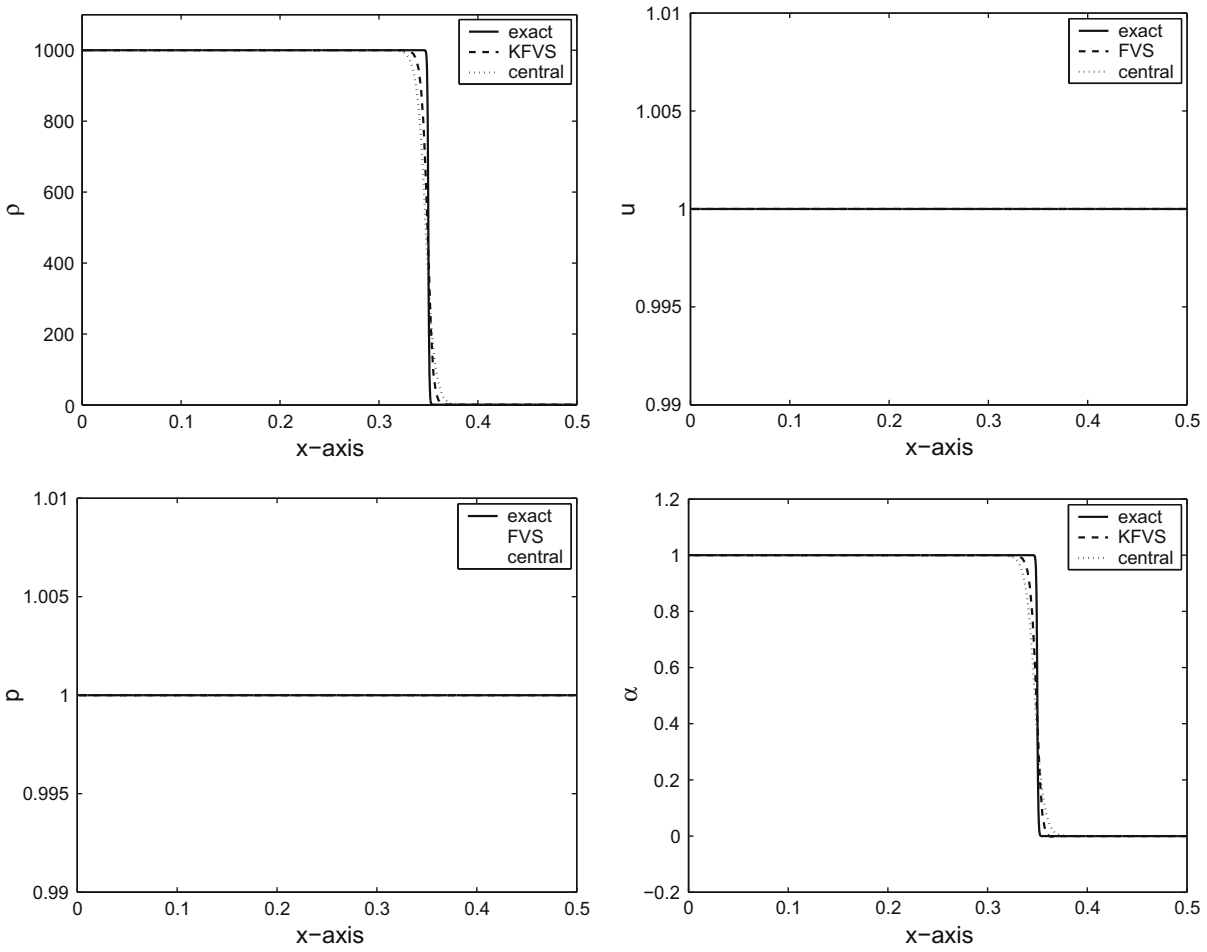

Fig. 2. Results of problem 1 on 200 mesh cells at $t = 0.1$.

5.2. Two-dimensional test problems

To test our numerical scheme for two-dimensional problems, two test cases are considered. We study the impact of a shock in air on a bubble of a lighter and a heavier gas, originally studied by Haas and Sturtevant [4]. The numerical compu-

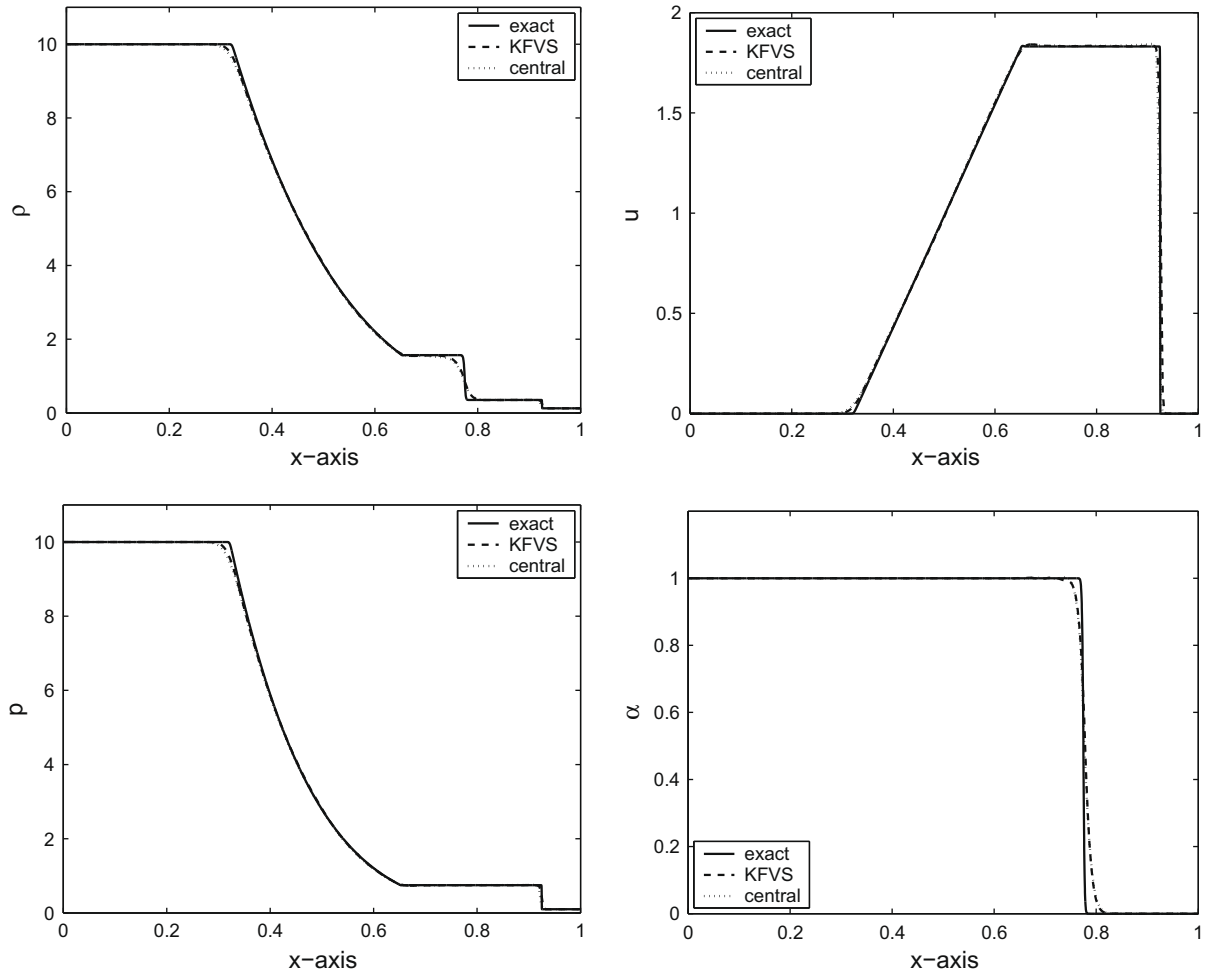

Fig. 3. Results of problem 1 on 300 mesh cells at $t = 0.015$.

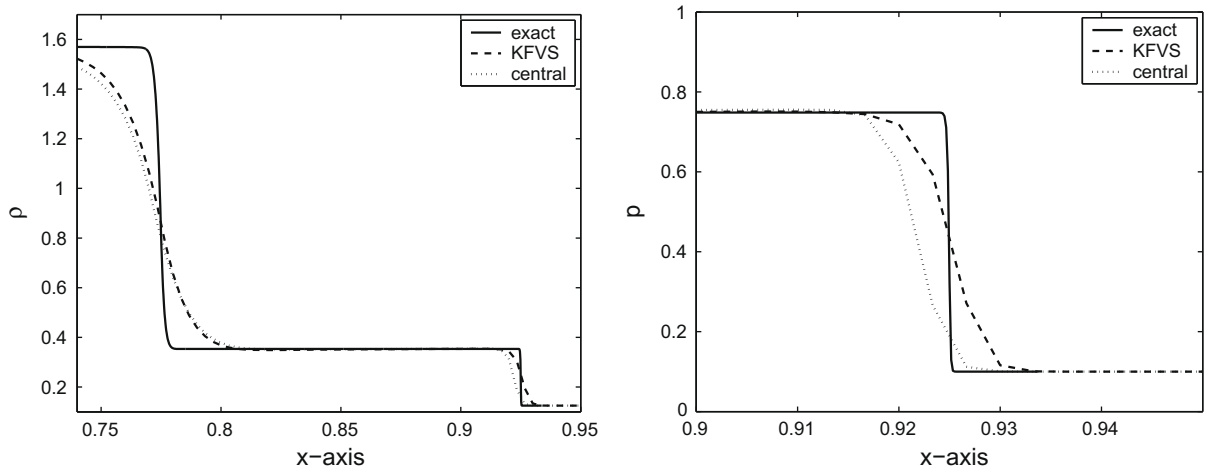

Fig. 4. Zoomed results of problem 2 on 300 mesh cells at $t = 0.015$.

tations are reported, among others, by Quirk and Karni [15], Marquina and Mulet [11], Kreeft and Koren [8], and Wackers and Koren [21]. A schematic computational setup is sketched in Fig. 1. We consider a shock tube of length 4.5 and width 0.89. The

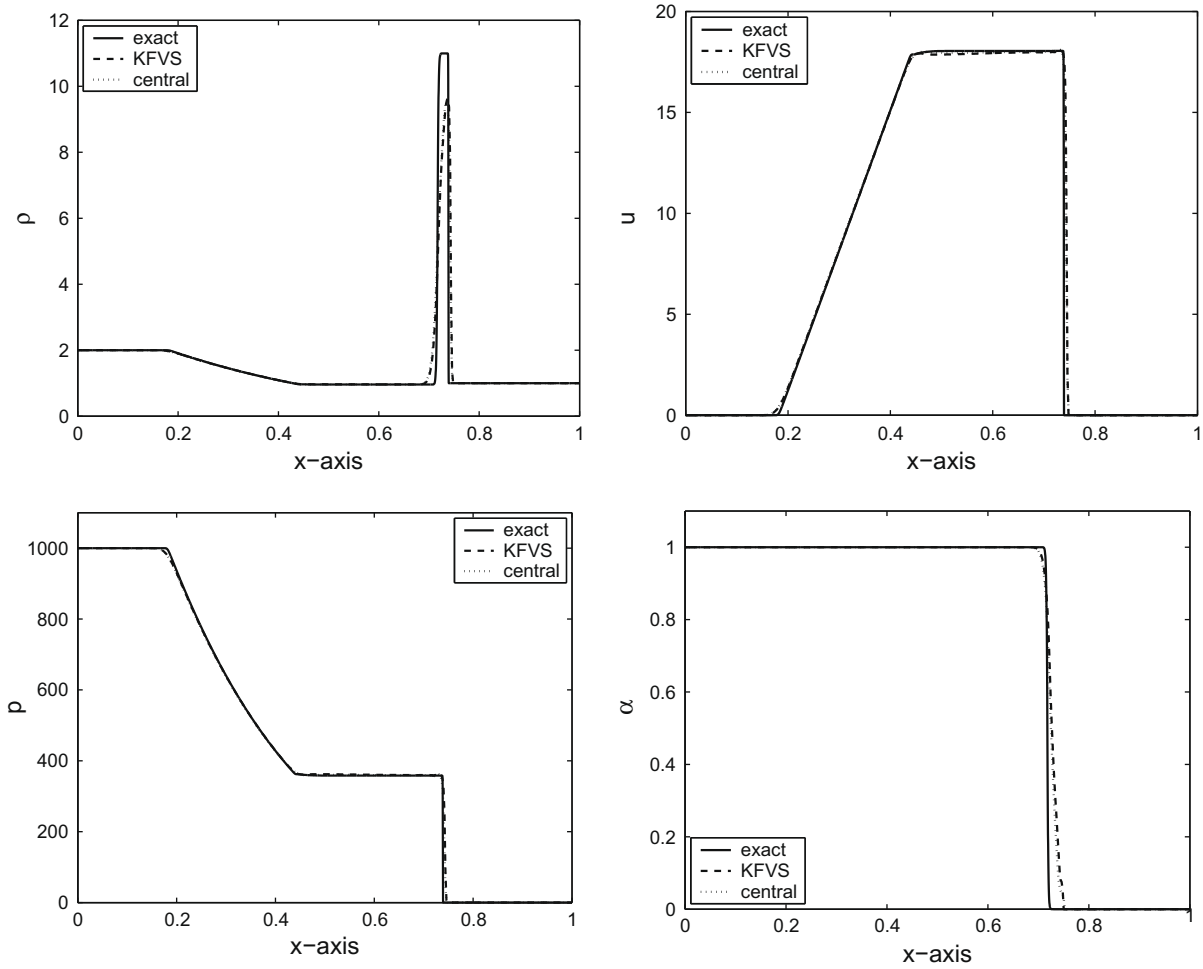

Fig. 5. Results of problem 2 on 500 mesh cells at $t = 0.012$.

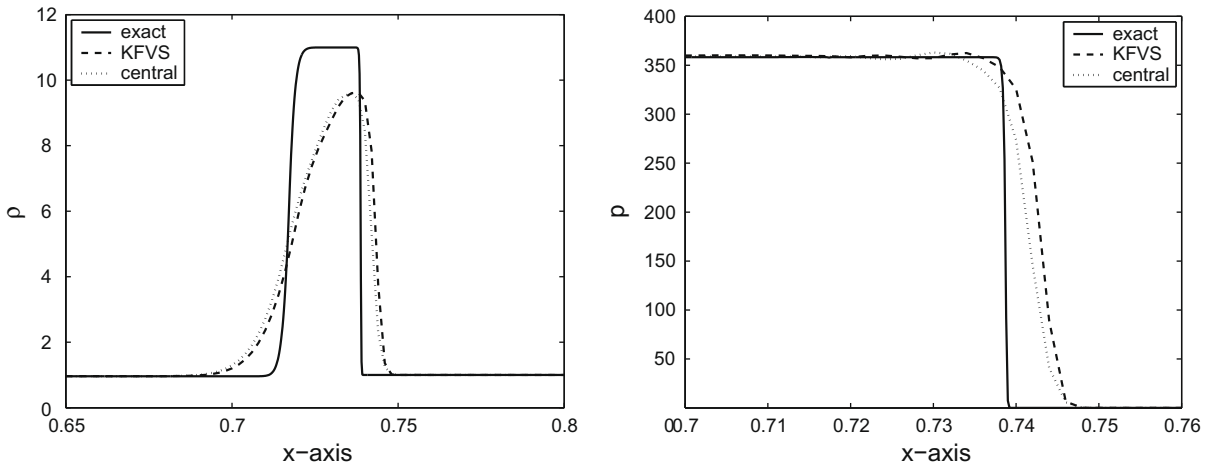

Fig. 6. Zoomed results of problem 3 on 500 mesh cells at $t = 0.012$.

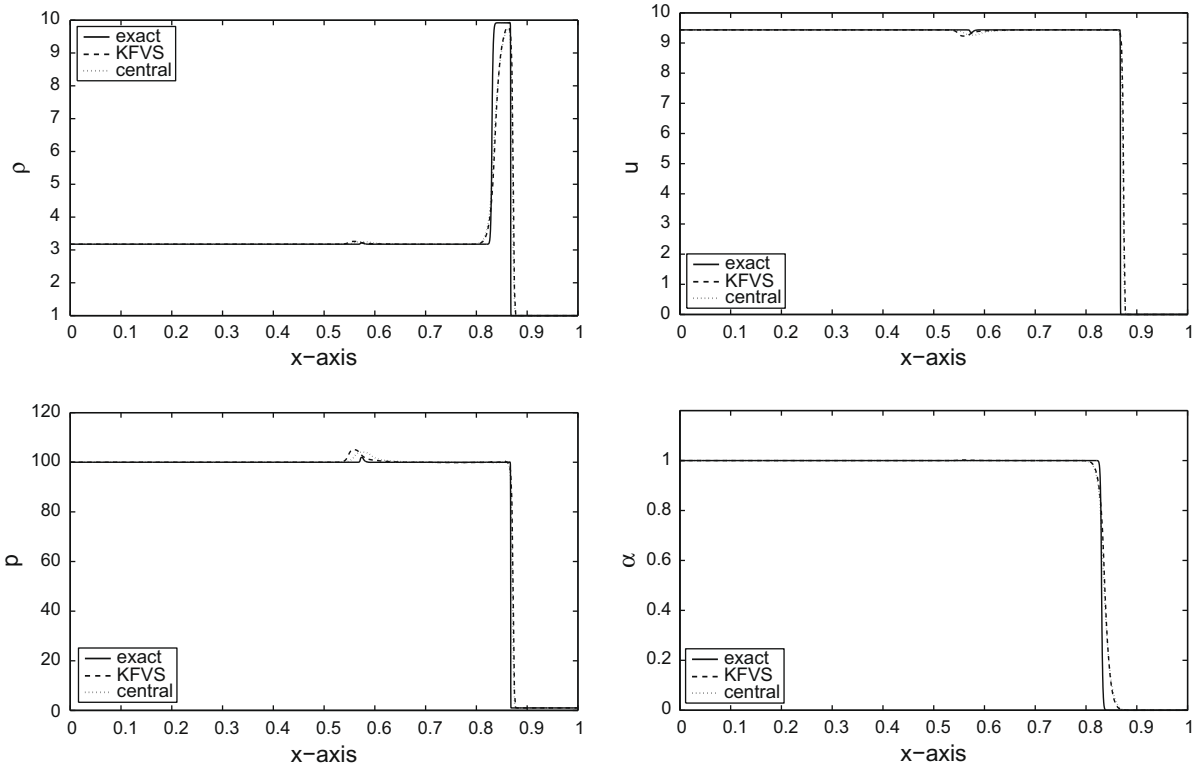

Fig. 7. Results of problem 4 on 400 mesh cells at $t = 0.015$.

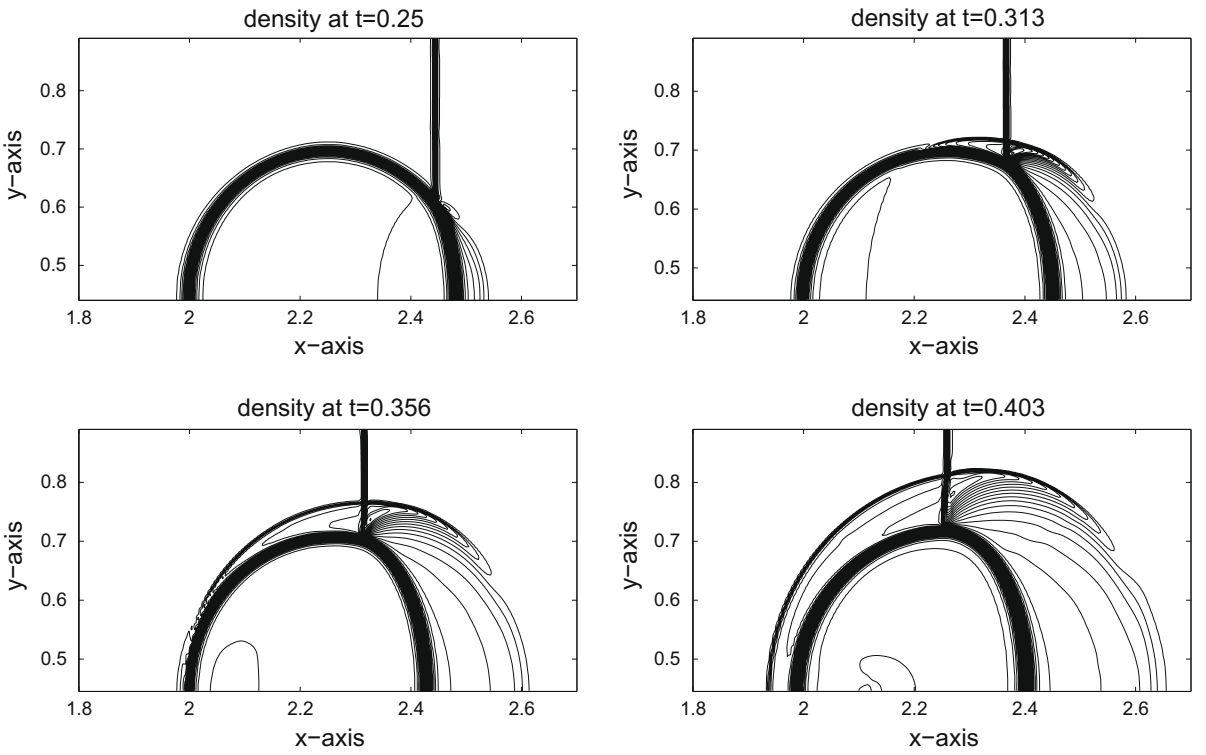

Fig. 8. Density contours of problem 5 (shock hitting helium bubble).

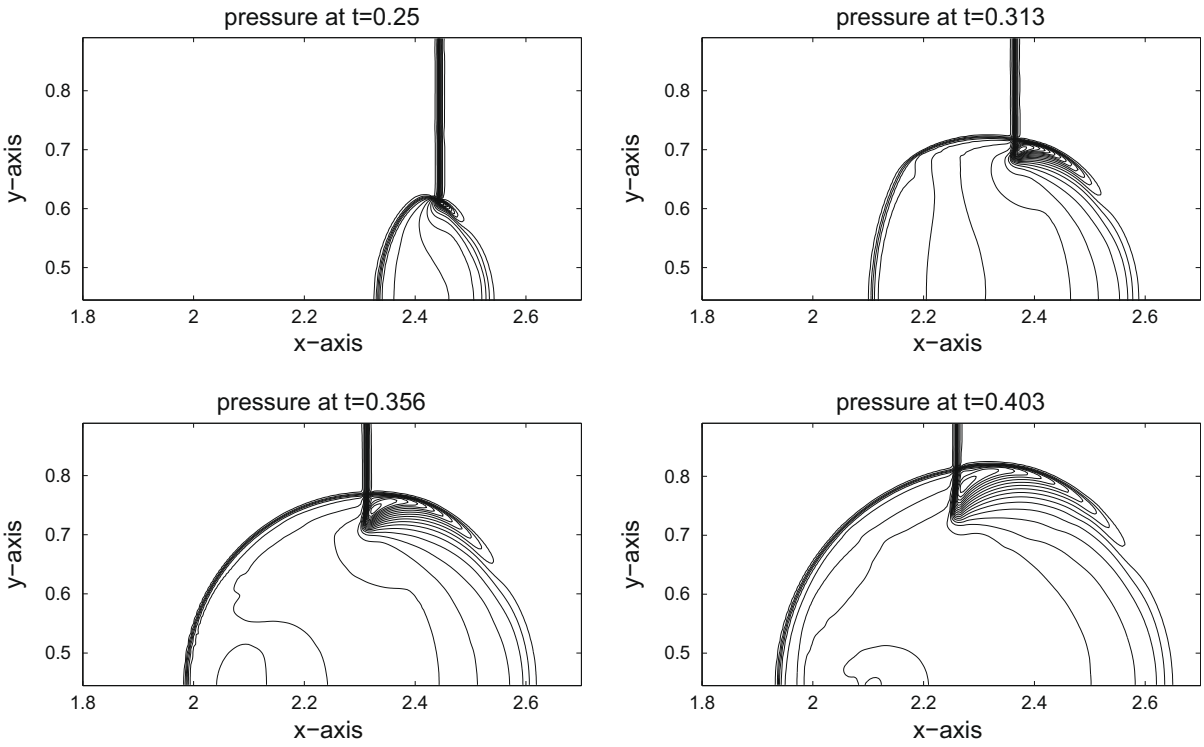

Fig. 9. Pressure contours of problem 5 (shock hitting helium bubble).

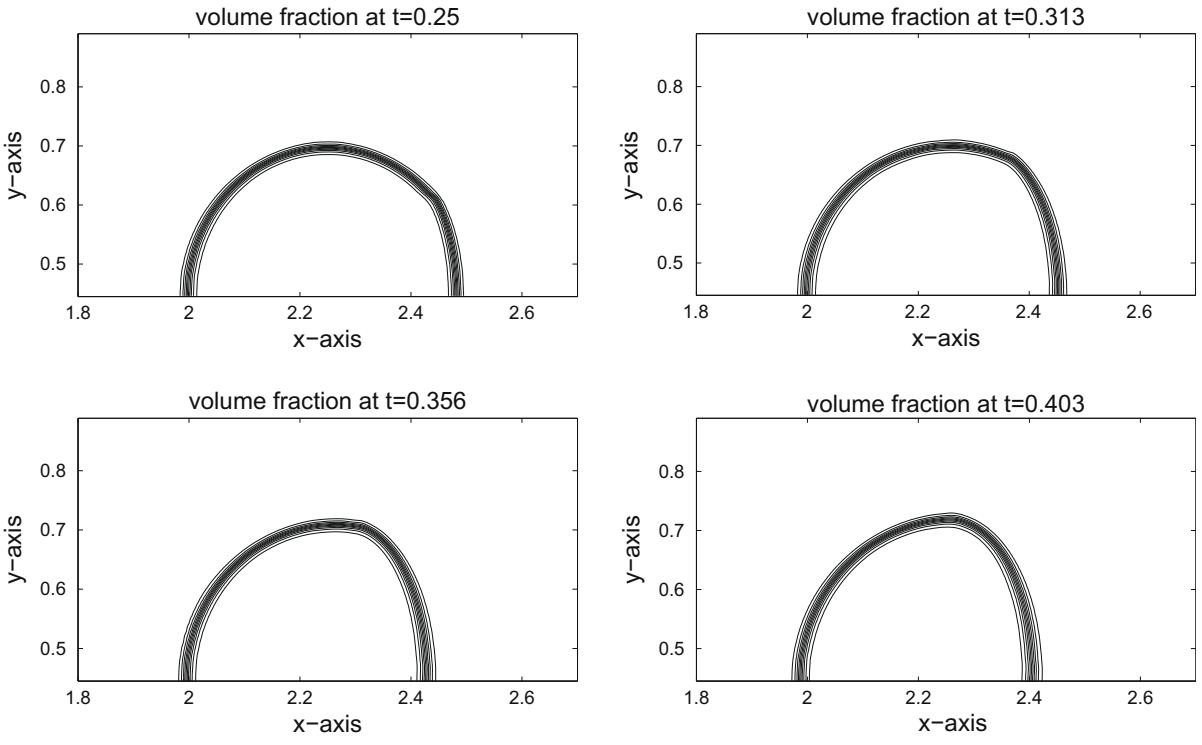

Fig. 10. Volume fraction contours of problem 5 (shock hitting helium bubble).

top and bottom walls of the tube are solid reflecting walls, while both ends of the tube are open. Inside the tube a cylinder of very thin cellular walls is placed. The cylinder is filled with some gas and then a shock wave is generated in the right end

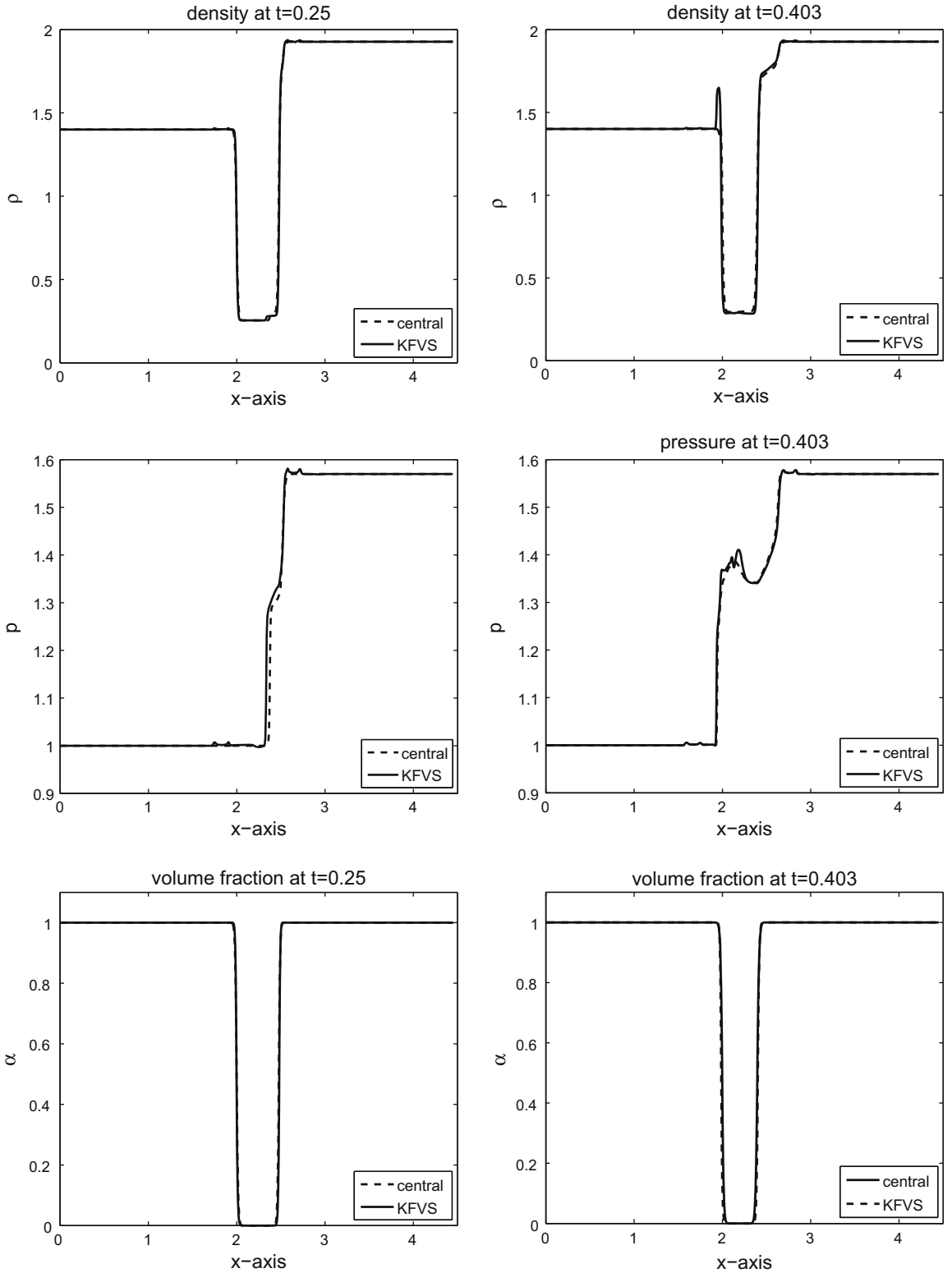

Fig. 11. One-dimensional plots along $y = 0.445$ for problem 5 (shock hitting helium bubble).

of the shock tube which is moving from right to left. After hitting by shock, the walls of the cylinder ruptures and the shock interacts with the gas of the cylinder. Due to fast interaction both gases do not mix in large amount, leading to a two-fluid flow problem. As the shock approaches to the surface of the bubble a reflected shock is generated from the surface of the bubble which moves towards right back in the air. At later time, this interaction become more and more complicated. The shock continues to move towards right in the air after passing through bubble and produces secondary reflected waves in the bubble when it hits the surface of the bubble.

Table 1
Comparison of velocities for helium bubble (problem 5).

	c_s (m/s)	c_r (m/s)	c_{ri} (m/s)
Present method	418	942	174
Quirk and Karni	422	943	178
Wackers and Koren	419	950	173
Experiments	410	900	170

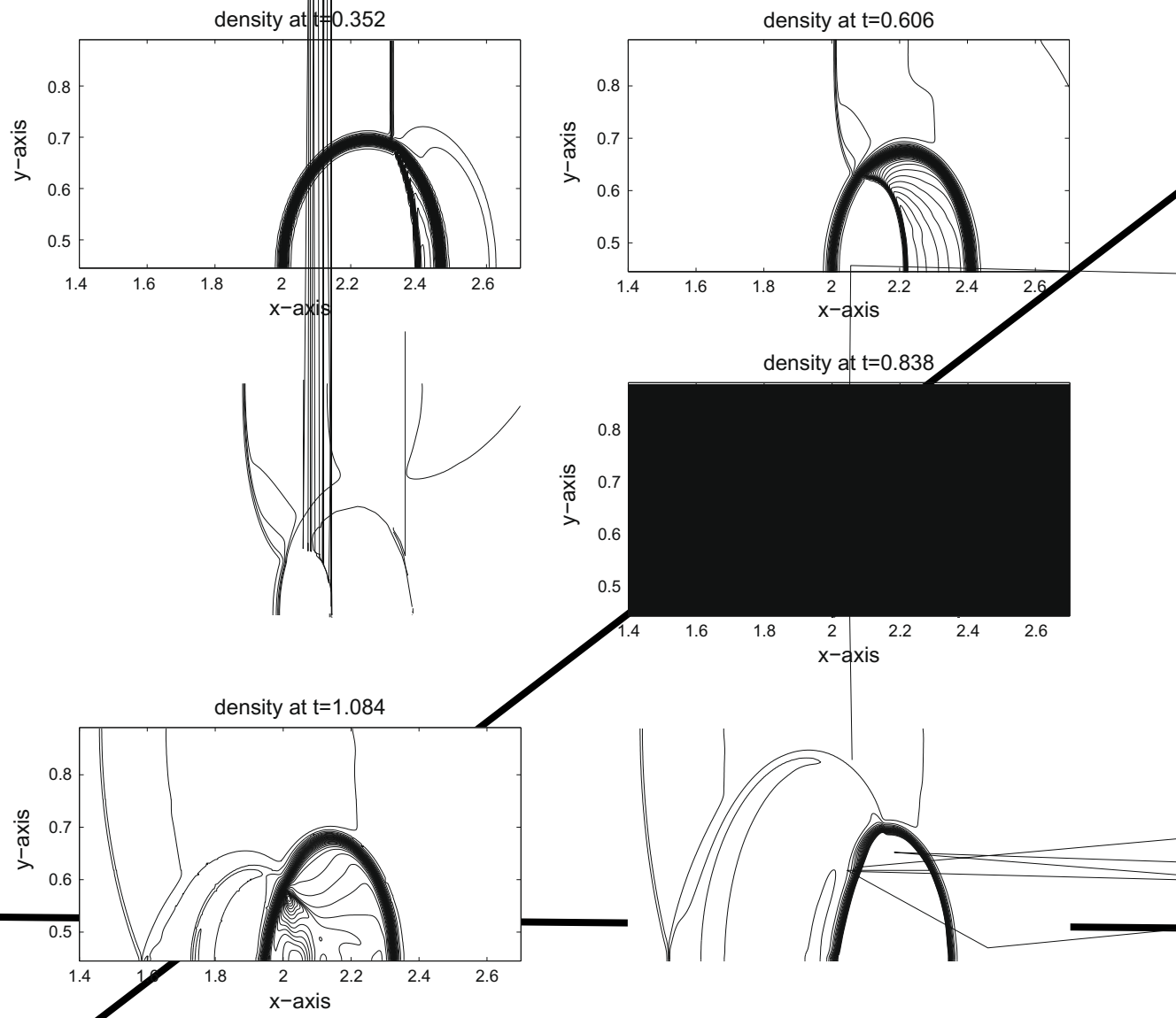

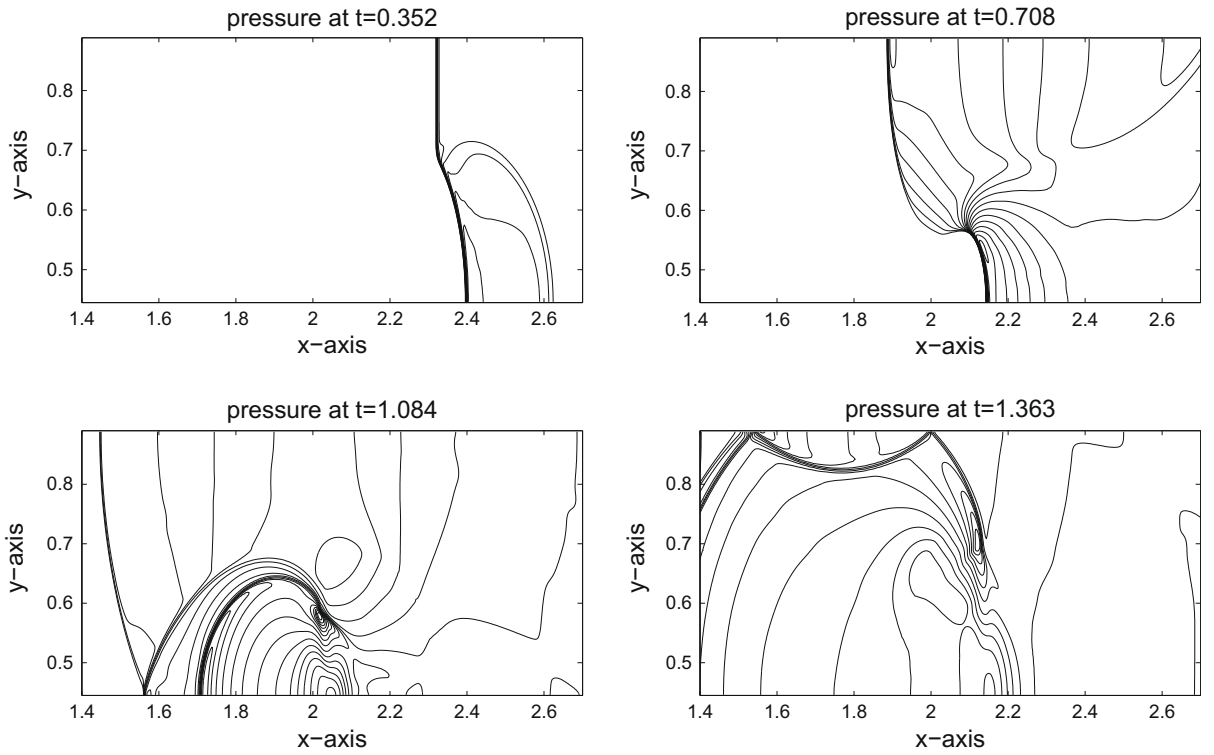

Fig. 13. Pressure contours of problem 6 (shock hitting R22 bubble).

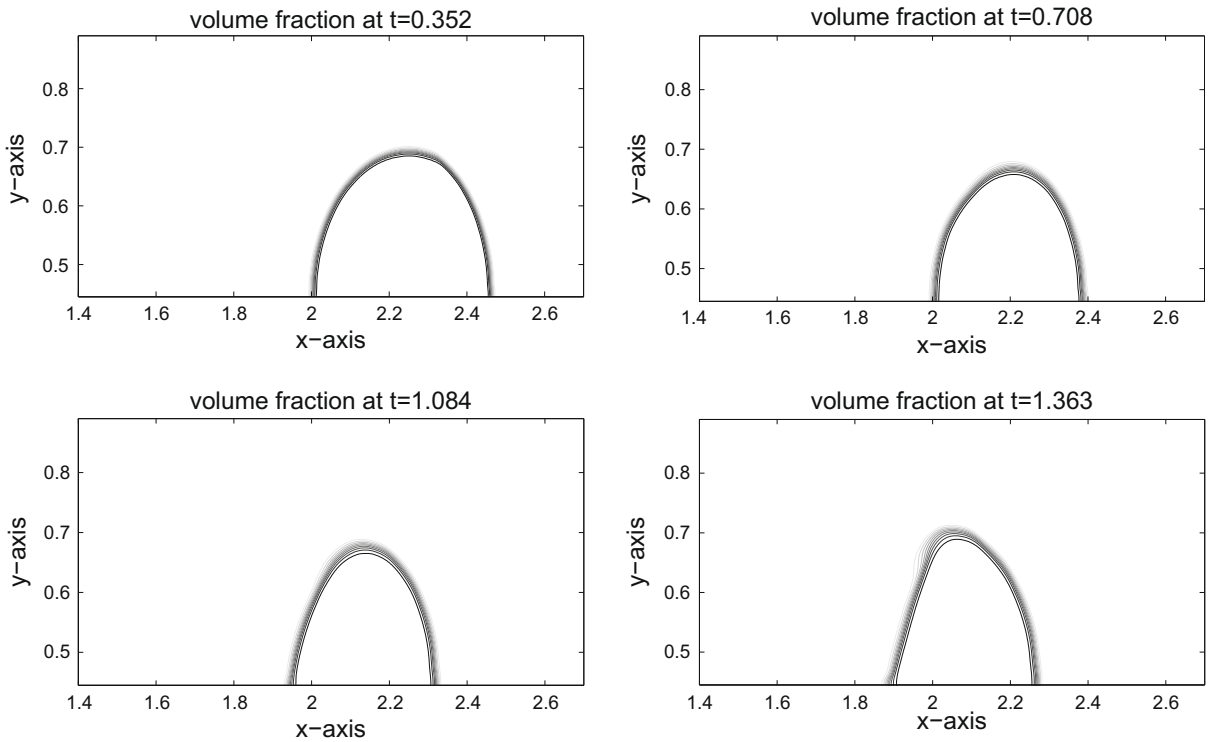

Fig. 14. Volume fraction contours of problem 6 (shock hitting R22 bubble).

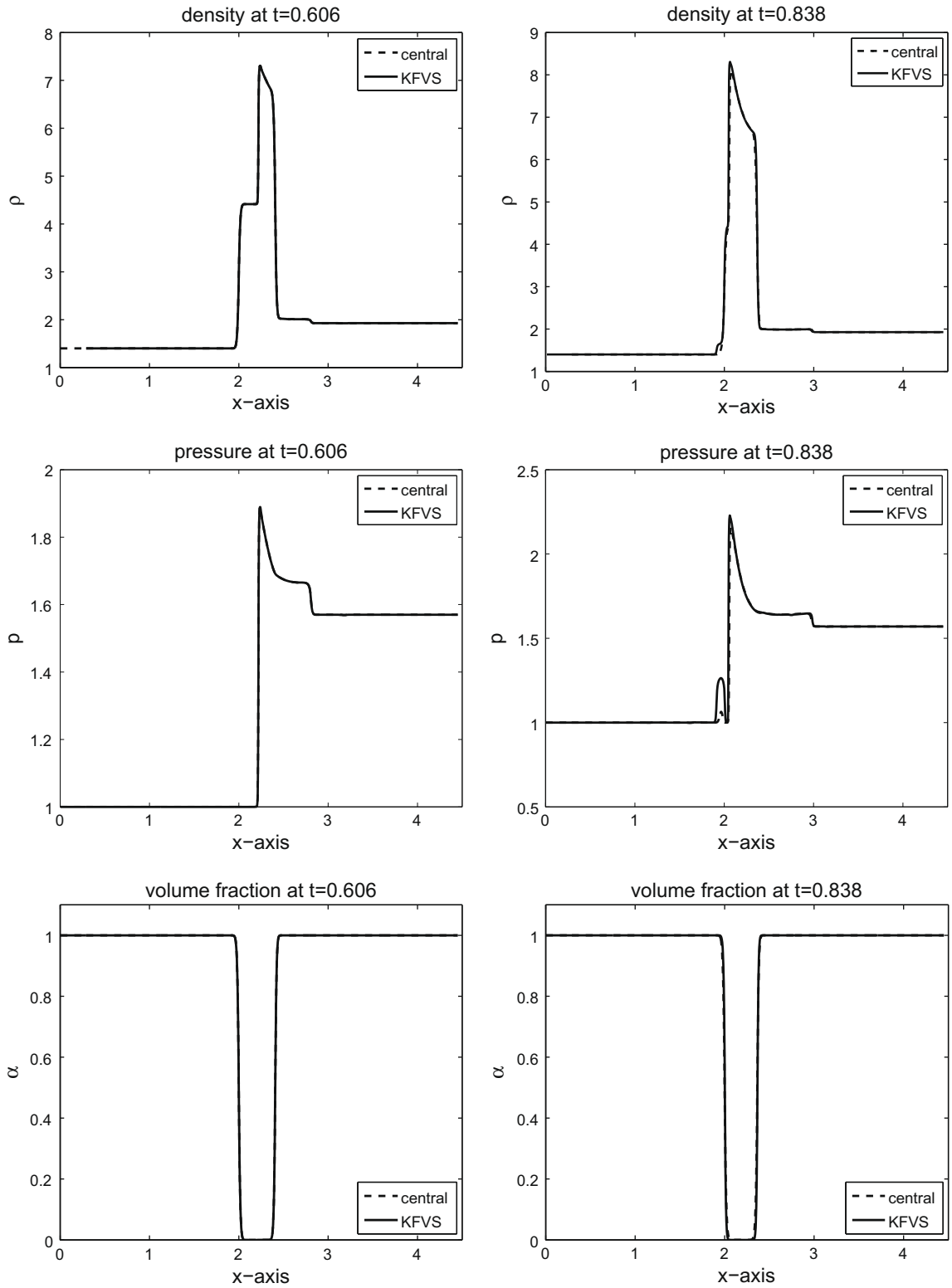

Fig. 15. One-dimensional plots along $y = 0.445$ for problem 6 (shock hitting R22 bubble).

The wave patterns generated by interaction are strongly depending on the density of the gas inside the bubble. However, some of the waves can be observed in all most all cases [21,8]. Here, a light helium gas and a heavy R22 gas are considered inside the cylindrical bubble.

Table 2
Comparison of volictiies for R22 bubble (problem 6).

	c_s (m/s)	c_r (m/s)	c_{ri} (m/s)
Present method	418	243	71
Quirk and Karni	420	254	70
Wackers and Koren	419	241	75
Experiments	415	240	73

Problem 5 (*Helium bubble*). In this example, we study the interaction of $Ms = 1.22$ planar shock, moving in air, with a cylindrical helium bubble contaminated with 28% of air. The bubble is assumed to be in thermodynamical and mechanical equilibrium with the surrounding air. The initial data are given as

$$(\rho, u, v, p, \gamma) = (1.40000, 0.0, 0.0, 1.0, 1.4), \quad \text{pre-shock air},$$
$$(\rho, u, v, p, \gamma) = (1.92691, -0.33361, 0.0, 1.5698, 1.4), \quad \text{post-shock air},$$
$$(\rho, u, v, p, \gamma) = (0.25463, 0.0, 0.0, 1.0, 1.648), \quad \text{helium}.$$

The position of key features occurred during the time evolution are well explained in [8,11,21]. Therefore, we omit discussion on these features. The computational domain is discretized into 1000×300 mesh cells. We display in Fig. 8 the contours of density at times: 0.25, 0.313, 0.356, 0.403. These results are closely matching with the plots given in [4,8,15,21] at times: 32 μs, 52 μs, 62 μs, 82 μs. The features used to match our contours with those in the literature are the relative position of some waves, such as refracted, transmitted or reflected shocks. Moreover, in Figs. 8 and 9 the contours of pressure and volume fraction show a perfect splitting of the pressure waves and the interface. The shocks and interface are sharp during the simulation. As observed by Wackers and Koren [21], the last interface is slowly bending inwards in Fig. 10. The phenomena will continue at later times until the bubble split in two vortices. The one-dimensional plots in Fig. 11, along the symmetry line $y = 0.445$, compare the results of KFVS and central schemes. Both schemes give comparable results.

Table 1 displays a quantitative comparison of present method with experiments of [4] and computations of [15,8,21]. In this table, c_{is} is the incident shock speed, c_r is the shock speed in bubble, and c_{ri} is the speed of the right side of two-fluid interface. The incident shock speed is given along the upper boundary of the computational domain, while the other two speeds are given along the centerline of the bubble ($y = 0.445$). The present results were scaled with a sound speed in air of 343 m/s, valid in air at sea level and at 293 K. Our results show a good agreement with available results.

Problem 6 (*R22 bubble*). Here, the same $Ms = 1.22$ planar shock moving in air hits a cylindrical R22 bubble which has higher density and lower ratio of specific heats than air. This results in about two times lower speed of sound. For more details on the key features the reader is referred to [8,21]. The initial data are given as

$$(\rho, u, v, p, \gamma) = (1.40000, 0.0, 0.0, 1.0, 1.4), \quad \text{pre-shock air},$$
$$(\rho, u, v, p, \gamma) = (1.92691, -0.33361, 0.0, 1.5698, 1.4), \quad \text{post-shock air},$$
$$(\rho, u, v, p, \gamma) = (4.41540, 0.0, 0.0, 1.0, 1.249), \quad \text{R22}.$$

The computational domain is discretized into 1000×300 mesh cells. Due to the lower speed of sound, the shock in the bubble and the refracted shock lag behind the incoming shock. Moreover, due to the circular shape of the bubble the refracted shock is curved. For the same reason, the reflected wave and shock wave are also curved. The contours of density are displayed in Fig. 12 at times: 0.352, 0.606, 0.708, 0.838, 1.084, 1.26. These results are closely matching with the plots given in [4,8,15,21] at times: 55 μs, 115 μs, 135 μs, 187 μs, 247 μs, 318 μs. Moreover, in Figs. 13 and 14 contour plots of pressure and volume fraction are given. The flow pattern observed in the density contours is split well in a pressure and the interface. Moreover, no wiggles are visible in our results and the pressure is continuous over the interface. Hence, the numerical results of our scheme reflect all key features as explained in [4,8,21]. The one-dimensional plots in Fig. 15, along the centerline $y = 0.445$, compare the results of KFVS and central schemes. It is clear from the plots that both schemes have comparable accuracy.

Finally, Table 2 display different speeds for R22 bubble. Once again, a good agreement can be seen with the already published results.

6. Conclusions

In this article, a high resolution KFVS scheme is derived for the numerical solution of a compressible two-fluid model of Wackers and Koren [21]. The proposed numerical scheme is based on the direct splitting of macroscopic flux-vector of the system of equations. In two space dimensions the scheme is implemented in a usual dimensionally split manner. The second order accuracy of the scheme is achieved by using MUSCL-type reconstruction and min-mod non-linear limiters. For validation, the results of the proposed numerical scheme are compared with those from the high resolution central scheme of Nessyahu and Tadmor [14]. A good agreement in the numerical results of both schemes was observed. However, it was found

that KFVS schemes gives better resolution of the sharp discontinuities compared to the central schemes. In both schemes, the non-differential part of the source terms were approximated by the cell averaged values. However, the differential parts of the source term are approximated similar to the convective fluxes. This work can be considered as a first step towards the approximation of the full seven-equation model by KFVS schemes. The seven-equation model is non-conservative and non-strictly hyperbolic. Therefore, this model usually gives hard time to a numerical scheme. The present experience with the reduced model will help us to solve the full seven-equation models more efficiently and accurately. Work is in progress in this direction and will be presented soon for publication.

Acknowledgment

A partial support from the Higher Education Commission of Pakistan at the COMSATS Institute of Information Technology Islamabad is gratefully acknowledged.

References

[1] R. Abgrall, R. Saurel, Discrete equations for physical and numerical compressible multiphase mixtures, J. Comp. Phys. 186 (2003) 361–396.
[2] G. Allaire, S. Clerc, S. Kokh, A five-equation model for the simulation of interfaces between compressible fluids, J. Comp. Phys. 181 (2002) 577–616.
[3] M.R. Baer, J.W. Nunziato, A two-phase mixture theory for the deflagration-to-detonation transition (DDT) in reactive granular materials, Int. J. Multiphase Flows 12 (1986) 861–889.
[4] J.F. Haas, B. Sturtevant, Interaction of weak shock waves with cylinderical and spherical gas inhomogeneities, J. Fluid Mech. 181 (1987) 41–76.
[5] A. Harten, P.D. Lax, B. Van Leer, On upstream differencing and Godunov-type schemes for hyperbolic conservation laws, SIAM Rev. 25 (1983) 35–62.
[6] C.W. Hirt, B.D. Nichols, Volume of fluid (VOF) method for the dynamics of free boundaries, J. Comp. Phys. 39 (1981) 201–225.
[7] G.-S. Jaing, E. Tadmor, Non-oscillatory central schemes for multidimensional hyperbolic conservation laws, SIAM J. Sci. Comput. 19 (1998) 1892–1917.
[8] J.J. Kreeft, B. Koren, A physical five-equation model for compressible two-fluid flow and its numerical treatment, CWI-Report MAS-E0905, Journal of Computational Physics, submitted for publication.
[9] S.F. Liotta, V. Romano, G. Russo, Central schemes for balance laws of relaxation type, SIAM J. Numer. Anal. 38 (2000) 1337–1356.
[10] J.C. Mandal, S.M. Deshpande, Kinetic flux-vector splitting for Euler equations, Comp. Fluids 23 (2) (1994) 447–478.
[11] A. Marquina, P. Mulet, A flux-split algorithm applied to conservative model for multicomponent compressible flows, J. Comp. Phys. 185 (2003) 120–138.
[12] W. Mulder, S. Osher, J.A. Sethian, Computing interface motion in compressible gas dynamics, J. Comp. Phys. 100 (1992) 209–228.
[13] A. Murrone, H. Guillard, A five-equation reduced model for compressible two phase flow problems, J. Comp. Phys. 202 (2002) 664–698.
[14] H. Nessyahu, E. Tadmor, Non-oscillatory central differencing for hyperbolic conservation laws, SIAM J. Comput. Phys. 87 (1990) 408–448.
[15] J.J. Quirk, S. Karni, On the dynamics of a shock-bubble interaction, J. Fluid Mech. 318 (1996) 129–163.
[16] R. Saurel, R. Abgrall, A multiphase Godunov method for compressible multifluids and multiphase flows, J. Comp. Phys. 150 (1999) 425–467.
[17] M. Sussman, P. Smereka, S. Osher, A level set approach for computing solutions to incompressible two-phase flow, J. Comp. Phys. 114 (1994) 146–159.
[18] T. Tang, K. Xu, A high-order gas-kinetic method for multidimensional ideal magnetohydrodynamics, J. Comp. Phys. 165 (2000) 69–88.
[19] H. Tang, T. Tang, K. Xu, A gas-kinetic scheme for shallow-water equations with source terms, Z. Angew. Math. Phys. (ZAMP) 55 (2004) 365–382.
[20] B. Van Leer, Flux vector splitting for the Euler equations, ICASE , Report No. 82-30, 1982.
[21] J. Wackers, B. Koren, Five-equation model for compressible two-fluid flow,Centrum Wiskunde & Informatica, CWI-Report MAS-E0414, 2004.
[22] J. Wackers, B. Koren, A fully conservative model for compressible two-fluid flow bubble, J. Numer. Meth. Fluids 47 (2005) 1337–1343.
[23] N.P. Weatherill, J.S. Mathur, M.J. Marchant, An upwind kinetic flux vector splitting method on general mesh topologies, Int. J. Numer. Meth. Eng. 37 (2) (1994) 623–643.
[24] K. Xu, Gas-kinetic theory based flux slitting method for ideal magneto-hydrodynamics, J. Comp. Phys. 153 (1999) 334–352.
[25] K. Xu, A well-balanced gas-kinetic scheme for the shallow-water equations with source terms, J. Comp. Phys. 178 (2002) 533–562.